LETTER

doi:10.1038/nature12972

Intestinal crypt homeostasis revealed at single-stem-cell level by *in vivo* live imaging

Laila Ritsma[1]*, Saskia I. J. Ellenbroek[1]*, Anoek Zomer[1], Hugo J. Snippert[2], Frederic J. de Sauvage[3], Benjamin D. Simons[4,5,6], Hans Clevers[1] & Jacco van Rheenen[1]

The rapid turnover of the mammalian intestinal epithelium is supported by stem cells located around the base of the crypt[1]. In addition to the Lgr5 marker, intestinal stem cells have been associated with other markers that are expressed heterogeneously within the crypt base region[1–6]. Previous quantitative clonal fate analyses have led to the proposal that homeostasis occurs as the consequence of neutral competition between dividing stem cells[7–9]. However, the short-term behaviour of individual Lgr5$^+$ cells positioned at different locations within the crypt base compartment has not been resolved. Here we establish the short-term dynamics of intestinal stem cells using the novel approach of continuous intravital imaging of Lgr5-Confetti mice. We find that Lgr5$^+$ cells in the upper part of the niche (termed 'border cells') can be passively displaced into the transit-amplifying domain, after the division of proximate cells, implying that the determination of stem-cell fate can be uncoupled from division. Through quantitative analysis of individual clonal lineages, we show that stem cells at the crypt base, termed 'central cells', experience a survival advantage over border stem cells. However, through the transfer of stem cells between the border and central regions, all Lgr5$^+$ cells are endowed with long-term self-renewal potential. These findings establish a novel paradigm for stem-cell maintenance in which a dynamically heterogeneous cell population is able to function long term as a single stem-cell pool.

In the small intestine, stem cells are associated with Lgr5 expression, which marks around 14–16 proliferative crypt base columnar (CBC) cells distributed throughout the crypt base. The stem-cell niche is constituted by Paneth cells[10,11] and the surrounding mesenchyme[12]. Cells that become displaced from this region enter the transit-amplifying domain (TA) and lose stemness[13]. Quiescent or slow-cycling cells, positioned at or near the +4 position may constitute a second stem-cell type[3,5,6,14], although a recent study indicated that some, if not all, of these cells represent secretory precursors that, in common with Dll1$^+$ cells higher in the crypt[15], can be recruited back into the stem-cell compartment upon damage[16]. The hierarchy, heterogeneity and spatial organization of intestinal stem cells remain subjects of debate[17–21]. It is unclear whether stem and progenitor cells are organized in an engrained proliferative hierarchy, defined by the signature of molecular markers, or whether stem cells transit reversibly between states of variable competence in which they become biased towards renewal or differentiation. If the latter is true, then it remains to be determined whether that bias is controlled by intrinsic heterogeneity in the expression of fate determinants, or is the consequence of spatiotemporal cues associated with niche-derived signals. Although inducible genetic lineage tracing allows us to dissect short-term heterogeneity in self-renewal potential, its reliability may be undermined by transient effects due to drug-inducing agents, Cre activity, or non-representativeness of labelling[22]. Therefore we applied an *in vivo* live-imaging strategy, allowing measurements to begin several days after drug administration. In common with previous live-imaging approaches used to study stem cells in hair follicle and testis[23–25], our approach enables tracing of the fate of individual marked stem cells and their progeny over time *in vivo*.

Multiphoton intravital microscopy and surgical implantation of an abdominal imaging window (AIW)[26,27] into living Lgr5$^{eGFP\text{-}Ires\text{-}CreERT2}$/R26R-Confetti mice were used to obtain visual access to the intestinal stem-cell niche (Fig. 1a). Lgr5$^+$ CBC cells and their progeny were lineage traced over time (Extended Data Fig. 1) by activating the expression of one of the Confetti colours (membranous cyan fluorescent protein (CFP), cytoplasmic yellow fluorescent protein (YFP) and red fluorescent protein (RFP)) in individual Lgr5$^+$ cells using tamoxifen-mediated recombination of the Confetti construct (Fig. 1a). To characterize the fate behaviour of CBC cells, we followed lineages of 80 marked cells ($n = 4$ mice) up to 5 days from the start of time-lapse imaging (Extended Data Fig. 2; for controls, see ref. 27 and Extended Data Fig. 3).

After induction, clonal progeny were observed throughout the stem-cell niche. To quantify the fate behaviour of Lgr5$^+$ CBC cells, we acquired z-stacks (Fig. 1b; see Supplementary Video 1 for the three-dimensional reconstruction) and classified cells based on their relative position, using the most basal cells (row 0) as a reference (Fig. 1b). Confetti-labelled clones were scored according to cell number, disaggregated by position (Extended Data Fig. 4). In line with predictions of neutral competition[7], numbers of marked cells in the stem-cell niche varied widely between clones (some expanded in size, others lost attachment to this compartment altogether; Extended Data Figs 2, 4). As just 1 of the 28 clones containing a single marked CBC cell at the start of filming remained single after 2 days of tracing, we chose to neglect the potential impact of lineage-committed quiescent Lgr5$^+$ cells, which was identified previously[16].

To investigate spatial heterogeneity in the self-renewal potential of CBC cells, we defined two regions within the Lgr5$^+$ stem-cell niche: a central (rows 0 to +2) and border (+3 and +4) region (Fig. 1b). A 'mother' cell in either the central or the border region could expand and give rise to progeny that extended into both regions (Fig. 1c–f and Extended Data Fig. 5). Further quantitative analysis was necessary to address the potency of CBC cells in these two domains. Although the average number of central cells per clone derived from a single central mother cell remained approximately constant, consistent with their maintenance over time, the average number of border cells derived from these cells increased to approximately two by day 3 (Fig. 2a). Furthermore, maintenance of the average central cell number was achieved through the steady decline in the number of clones retaining at least one central cell (Fig. 2b), compensated by a steady increase in size of those that remained (Fig. 2c). Although clones derived from single border mother cells also appeared to approximately maintain their number, they gave rise to a comparatively smaller number of central cells (Fig. 2a). The sustained increase in the number of border cells from a central

[1]Cancer Genomics Netherlands, Hubrecht Institute-KNAW and University Medical Centre Utrecht, Uppsalalaan 8, 3584 CT Utrecht, The Netherlands. [2]University Medical Centre Utrecht, Universiteitsweg 100, 3584 CG Utrecht, The Netherlands. [3]Department of Molecular Biology, Genentech Inc., 1 DNA Way, South San Francisco, California 94080, USA. [4]Cavendish Laboratory, Department of Physics, J. J. Thomson Avenue, University of Cambridge, Cambridge CB3 0HE, UK. [5]The Wellcome Trust/Cancer Research UK Gurdon Institute, University of Cambridge, Tennis Court Road, Cambridge CB2 1QN, UK. [6]The Wellcome Trust/Medical Research Council Stem Cell Institute, University of Cambridge, Tennis Court Road, Cambridge CB2 1QN, UK.

*These authors contributed equally to this work.

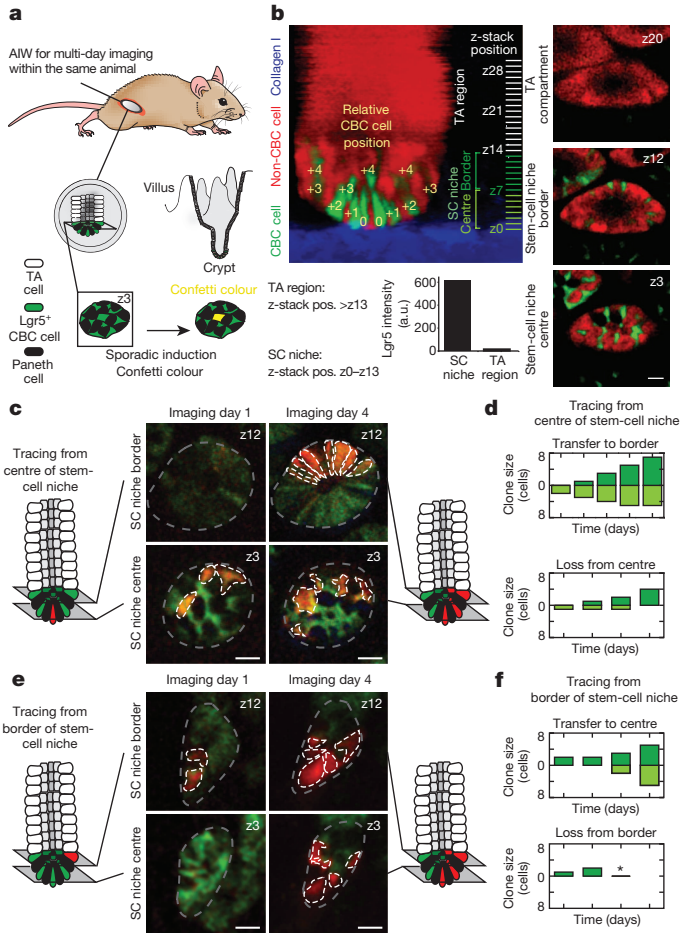

Figure 1 | Intravital lineage tracing of Lgr5^{+} cells. **a**, Cartoon showing a Lgr5$^{eGFP\text{-}Ires\text{-}CreERT2}$/R26R-Confetti mouse with an AIW to visualize intestinal Lgr5^{+} CBC cells and their Confetti progeny over multiple imaging sessions. **b**, Lateral projection of a z-stack and representative *xy* images of a crypt at indicated z-stack positions (pos.). The stem-cell (SC) niche (z0–13) is defined by Lgr5–GFP fluorescence. The relative position of CBC cells to the most basal cell (row 0) determines location in the central (row 0 to +2, which translates to z0–6) or border region (row +3 to +4, which translates to z7–13) of the stem-cell niche. a.u., arbitrary units. Scale bar, 20 μm. **c**–**f**, Intravital lineage tracing of RFP-expressing Lgr5^{+} CBC cells located at the centre (**c**, **d**) and border (**e**, **f**) regions. Grey lines indicate crypts, white lines indicate Confetti clones. **d**, **f**, Graphs show time evolution of spatial organization of Confetti clones starting 3 days after induction. Clone size is divided into central (light green) and border (dark green) CBC cells. Asterisk indicates clones in which all progeny were lost. Scale bar, 20 μm.

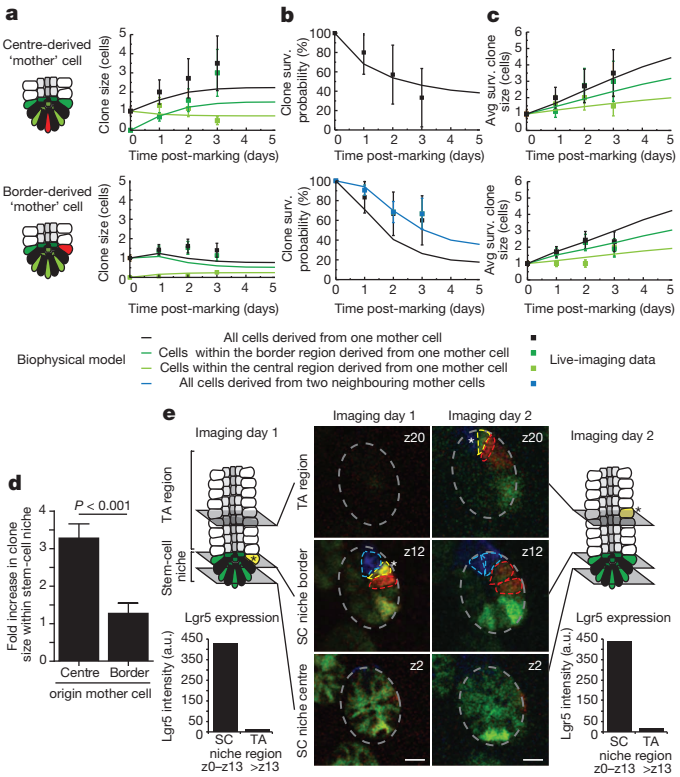

Figure 2 | Central CBC cells experience a short-term positional advantage in self-renewal potential. **a**–**c**, Clonal evolution of a Confetti cell located at the central or border region starting 3 days after induction. Graphs show average clone size (**a**), fraction of 'surviving' clones that contain at least one marked central (top) or border (bottom) cell (**b**), and average size of surviving clones (clones with at least one marked cell) (**c**). Different colours indicate different regions in the niche. Points show data and lines show fit to the biophysical model (see Fig. 3). Error bars represent standard deviation (s.d.). **d**, Fold increase in clone size over 3 days from a border or central Confetti^{+} CBC cell. Note that central stem cells have a positional advantage over border stem cells. Error bars represent standard error of the mean (s.e.m.); $P < 0.001$ obtained using a Mann–Whitney U test. **e**, Intravital images of the same crypt at indicated times. Note that the yellow cell is truly expelled from the stem-cell (SC) niche, as GFP expression was absent in the TA cell region (see charts at indicated time points). Scale bars, 20 μm.

mother cell (Fig. 2a) indicates that these cells typically outcompete cells at the niche border (Fig. 2d).

To investigate the potential basis of this positional advantage, we studied the development of clones with finer time resolution. Every 2 hours, we acquired multiphoton images of crypts, followed the location of all green fluorescent protein (GFP)-labelled cells over time (Extended Data Fig. 6 and Supplementary Videos 2–4), and found that division of single Lgr5^{+} cells coincides with displacement of proximate CBC cells. This suggests that cell proliferation creates competition for space, leading to an adjustment of cell positions. Through this rearrangement, and independent of their division history, CBC cells located at the border can become passively displaced from the niche after division of a neighbour (Fig. 2e and Extended Data Fig. 4).

To challenge this conclusion and address the potency of the Lgr5^{+} CBC stem-cell population, we aimed to capture quantitatively the variability seen in the lineage potential of individual cells by a biophysical model, involving a revision of the neutral drift dynamics model introduced previously[7,8], in which all stem cells were considered functionally equivalent. In this new model, a periodic quasi-one-dimensional arrangement of stem cells mimicked the 'collar-like' geometry of the central and border niche regions of the crypt (Fig. 3a). To account for the mixed GFP expression profile seen at rows +3 and +4 (Fig. 1b), the border region was further subdivided into Lgr5^{+} CBC cells and Lgr5^{-} TA cells. To accommodate the range of observed dynamical behaviours in the stem-cell niche, we allowed for five possible 'channels' of stem-cell loss and replacement (Fig. 3a). That is, after division of a border stem cell, one daughter cell remains at its position while the other either (1) displaces a border TA cell out of the niche; (2) displaces a border stem cell that in turn displaces a border TA cell out of the niche; or (3) displaces a central stem cell that in turn displaces a border stem cell into the border TA cell domain. Similarly, after division of a central stem cell, one daughter remains at its position while the other either (4) displaces a border stem cell into the border TA cell region; or (5) displaces a central cell that in turn displaces a border stem cell into the TA cell region. If we define λ as the rate of transfer of border TA cells out of the niche, each of these five processes occur at rates $P_b\lambda$, $P_{bb}\lambda$, $P_{bc}\lambda$, $P_{cb}\lambda$ and $P_{cc}\lambda$, respectively, with $P_b + P_{bb} + P_{bc} + P_{cb} + P_{cc} = 1$ (Supplementary Notes).

By fixing the relative rates of stem-cell division and displacement by the observed average clone size dependences and independent estimates

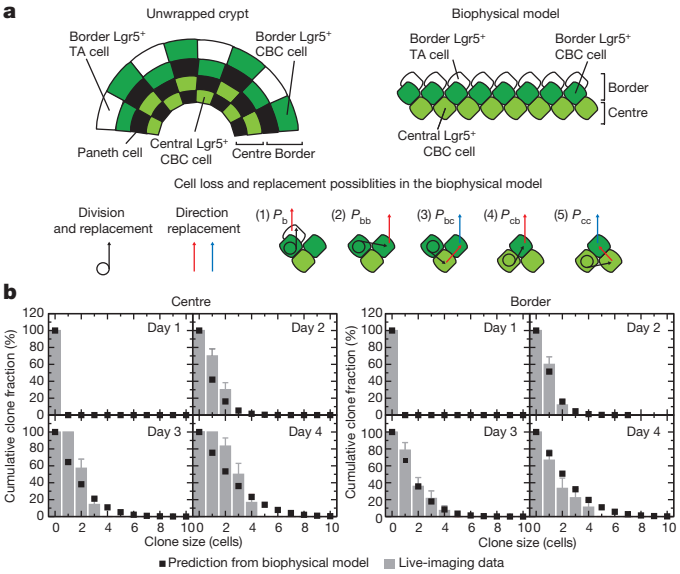

Figure 3 | Biophysical model of intestinal stem-cell dynamics. **a**, From the unfolded crypt caricature (left), we synthesize a quasi-one-dimensional biophysical model of the niche region (right) consisting of two domains: border and centre. To conserve cell number, cell rearrangements after stem-cell division displace precisely one cell from the border. To capture the range of lineage data, we include five channels of stem-cell loss/replacement (1–5), as defined in the main text. **b**, Cumulative size distributions of clones derived from a single cell in the centre (left) or border (right). Clone size is defined in both cases by total number of constituent cells in the centre and border regions. Error bars represent s.e.m. Points represent predictions of the model using the same parameters as those inferred from the average dependences (Supplementary Notes).

of the average cell division rate, we found that the biophysical model can accurately predict the clone size distribution and spatial dependencies observed in live imaging (Figs 2a–c, 3b and Extended Data Fig. 7). More significantly, with the same parameters, the model describes quantitatively convergence onto the hallmark scaling behaviour reported using static lineage tracing assays at intermediate times[7] (7 and 14 days after induction), as well as the predicted progression towards crypt monoclonality at long times[8] (Extended Data Figs 8, 9 and Supplementary Notes).

To challenge the model further, we traced the recovery of stem cells after targeted ablation of Lgr5$^+$ cells using diphtheria toxin (DT) injection in mice in which the human DT receptor (DTR) fused to enhanced (e)GFP was knocked in at the *Lgr5* locus (Lgr5$^{DTR:eGFP}$)[28] (Fig. 4a). In these mice, recovered Lgr5$^+$ cells are derived from a TA lineage[28]. After complete depletion (Fig. 4a), we observed a low frequency of initiation and a heterogeneous pattern of recovery (Fig. 4b and Supplementary Video 5), suggesting sporadic transfer of cells from the TA zone into the stem-cell niche border. The cohesion of these recovered cell clusters (Supplementary Video 6) suggests clonal expansion of individual TA cells. Intriguingly, by allowing individual border stem cells to recolonize a depleted stem-cell niche through cell division uncompensated by loss, our biophysical model provided a quantitative prediction of cluster composition (border versus central) by size, with the same relative rates of stem-cell division as those found in the steady state (Fig. 4c and Supplementary Notes).

Our data show that intestinal stem-cell maintenance follows from competition between proximate CBC stem cells for limited niche access, and that stem cells positioned near the niche boundary experience a bias towards loss and replacement, whereas stem cells remote from the boundary are biased towards survival. Intriguingly, a similar dependence of self-renewal potential on proximity to the niche border was reported in a recent *in vivo* live-imaging study of the mouse hair follicle[29], suggesting that such heterogeneity may be a ubiquitous feature of adult stem-cell populations. A recent lineage tracing study based on the continuous and sporadic acquisition of mutations during DNA replication concluded that only a subfraction of putative intestinal stem cells are 'functional'[30]. Our quantitative analysis of live-imaging data shows that central stem cells are about three times more likely than border cells to colonize fully a crypt in steady state, explaining why only a fraction of Lgr5$^+$ cells seem to retain long-term self-renewal

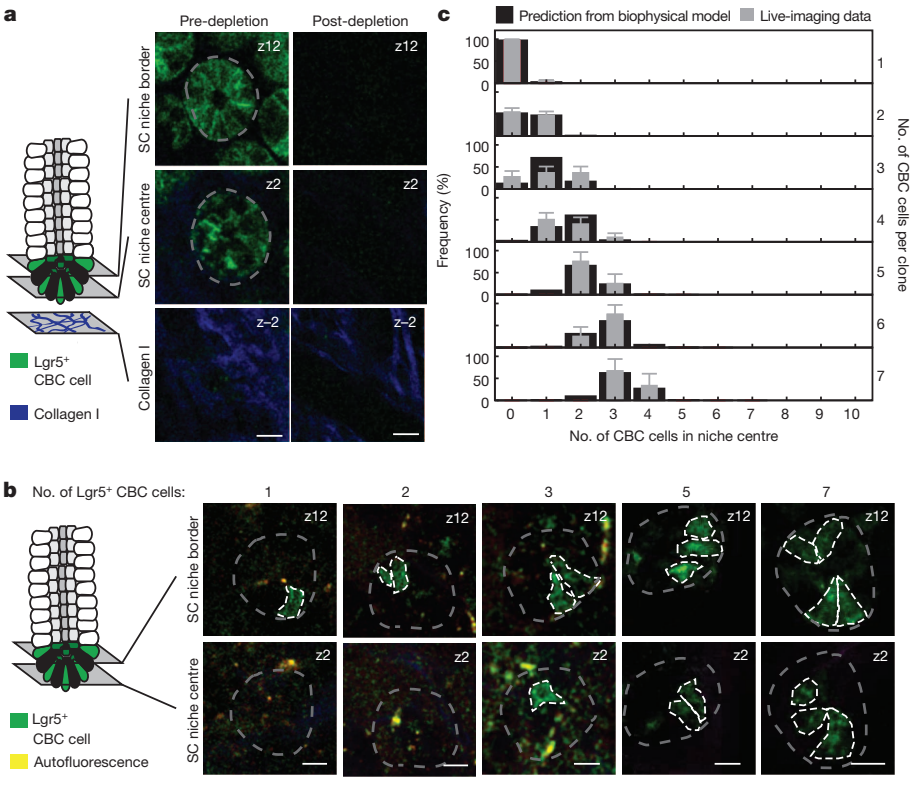

Figure 4 | Recovery of stem-cell compartment after ablation of Lgr5$^+$ cells challenges model. **a**, Targeted ablation of Lgr5$^+$ cells in Lgr5$^{DTR:eGFP}$ mice was induced by injection of DT. Shown are representative images pre- and post-ablation. Scale bars, 20 μm. **b**, Recovery of Lgr5$^+$ CBC cells was monitored only in mice in which full depletion was confirmed 24 h after DT injection. Images taken at 72 h after depletion show representative crypts containing clonal clusters of different sizes ($n = 108$ crypts in 3 mice). Scale bars, 20 μm. **c**, For all various clone sizes, measured spatial composition (border versus centre) of Lgr5$^+$ CBC cells in clusters (grey) was accurately predicted by the biophysical model (black). Error bars represent s.d.

potential (Supplementary Notes). Through the transfer of cells between the central and border regions of the niche, the dynamic and heterogeneous population of intestinal stem cells is able to function long term as a single equipotent pool.

METHODS SUMMARY

All experiments were carried out in accordance with the guidelines of the Animal Welfare Committee of the Royal Netherlands Academy of Arts and Sciences. $Lgr5^{eGFP\text{-}Ires\text{-}CreERT2}$/R26R-Confetti mice between 10 and 22 weeks old were used for experiments. Three days before imaging, mice were injected with 2.5–5 mg tamoxifen (Sigma Aldrich) to activate expression of Confetti colours. $Lgr5^{DTR:eGFP}$ mice with an AIW received 50 $\mu g\,kg^{-1}$ DT through intraperitoneal injections. Intravital imaging was performed on an inverted Leica TCS SP5 AOBS two-photon microscope with a chameleon Ti:Sapphire pumped optical parametric oscillator (Coherent) equipped with a ×25 (HCX IRAPO NA0.95 WD 2.5 mm) water objective and four non-descanned detectors (NDDs). Confetti colours were detected using sequential scanning: excitation 860 nm, NDD2 455–490 nm emission (CFP and eGFP); excitation 960 nm, NDD3 500–550 nm emission (eGFP and YFP), NDD4 560–650 nm emission (YFP and RFP). Second harmonic generation (SHG) signal was generated by 960 nm excitation at collagen I and detected in NDD2. z-stacks with 2.5 μm z-steps of typically 70–80 images were acquired. Re-identification of the same crypts over multiple days was accomplished by storing the *xy* coordinates of the imaged regions using the 'multiple position' function in the LAS-AF software and using the vasculature and the typical $Lgr5^{+}$ crypt pattern as visual landmarks. Acquired images were processed using a custom-designed Visual Basic program and further processed with ImageJ (National Institutes of Health).

Online Content Any additional Methods, Extended Data display items and Source Data are available in the online version of the paper; references unique to these sections appear only in the online paper.

Received 30 May; accepted 20 December 2013.
Published online 16 February 2014.

1. Barker, N. *et al.* Identification of stem cells in small intestine and colon by marker gene *Lgr5*. *Nature* **449,** 1003–1007 (2007).
2. Sangiorgi, E. & Capecchi, M. R. *Bmi1* is expressed *in vivo* in intestinal stem cells. *Nature Genet.* **40,** 915–920 (2008).
3. Takeda, N. *et al.* Interconversion between intestinal stem cell populations in distinct niches. *Science* **334,** 1420–1424 (2011).
4. Montgomery, R. K. *et al.* Mouse telomerase reverse transcriptase (mTert) expression marks slowly cycling intestinal stem cells. *Proc. Natl Acad. Sci. USA* **108,** 179–184 (2011).
5. Powell, A. E. *et al.* The Pan-ErbB negative regulator Lrig1 is an intestinal stem cell marker that functions as a tumor suppressor. *Cell* **149,** 146–158 (2012).
6. Wong, V. W. Y. *et al.* Lrig1 controls intestinal stem-cell homeostasis by negative regulation of ErbB signalling. *Nature Cell Biol.* **14,** 401–408 (2012).
7. Snippert, H. J. *et al.* Intestinal crypt homeostasis results from neutral competition between symmetrically dividing Lgr5 stem cells. *Cell* **143,** 134–144 (2010).
8. Lopez-Garcia, C., Klein, A. M., Simons, B. D. & Winton, D. J. Intestinal stem cell replacement follows a pattern of neutral drift. *Science* **330,** 822–825 (2010).
9. Snippert, H. J. & Clevers, H. Tracking adult stem cells. *EMBO Rep.* **12,** 113–122 (2011).
10. Sato, T. *et al.* Paneth cells constitute the niche for Lgr5 stem cells in intestinal crypts. *Nature* **469,** 415–418 (2011).
11. VanDussen, K. L. *et al.* Notch signaling modulates proliferation and differentiation of intestinal crypt base columnar stem cells. *Development* **139,** 488–497 (2012).
12. Farin, H. F., Van Es, J. H. & Clevers, H. Redundant sources of Wnt regulate intestinal stem cells and promote formation of Paneth cells. *Gastroenterology* **143,** 1518–1529 (2012).
13. van der Flier, L. G. & Clevers, H. Stem cells, self-renewal, and differentiation in the intestinal epithelium. *Annu. Rev. Physiol.* **71,** 241–260 (2009).
14. Sangiorgi, E. & Capecchi, M. R. Bmi1 lineage tracing identifies a self-renewing pancreatic acinar cell subpopulation capable of maintaining pancreatic organ homeostasis. *Proc. Natl Acad. Sci. USA* **106,** 7101–7106 (2009).
15. van Es, J. H. *et al.* $Dll1^{+}$ secretory progenitor cells revert to stem cells upon crypt damage. *Nature Cell Biol.* **14,** 1099–1104 (2012).
16. Buczacki, S. J. A. *et al.* Intestinal label-retaining cells are secretory precursors expressing Lgr5. *Nature* **495,** 65–69 (2013).
17. Stine, R. R. & Matunis, E. L. Stem cell competition: finding balance in the niche. *Trends Cell Biol.* **23,** 357–364 (2013).
18. Simons, B. D. & Clevers, H. Strategies for homeostatic stem cell self-renewal in adult tissues. *Cell* **145,** 851–862 (2011).
19. Morrison, S. J. & Spradling, A. C. Stem cells and niches: mechanisms that promote stem cell maintenance throughout life. *Cell* **132,** 598–611 (2008).
20. Goulas, S., Conder, R. & Knoblich, J. A. The Par complex and integrins direct asymmetric cell division in adult intestinal stem cells. *Cell Stem Cell* **11,** 529–540 (2012).
21. Sheng, X. R. & Matunis, E. Live imaging of the *Drosophila* spermatogonial stem cell niche reveals novel mechanisms regulating germline stem cell output. *Development* **138,** 3367–3376 (2011).
22. Zhu, Y., Huang, Y.-F., Kek, C. & Bulavin, D. V. Apoptosis differently affects lineage tracing of Lgr5 and Bmi1 intestinal stem cell populations. *Cell Stem Cell* **12,** 298–303 (2013).
23. Nakagawa, T., Sharma, M., Nabeshima, Y.-i., Braun, R. E. & Yoshida, S. Functional hierarchy and reversibility within the murine spermatogenic stem cell compartment. *Science* **328,** 62–67 (2010).
24. Klein, A. M., Nakagawa, T., Ichikawa, R., Yoshida, S. & Simons, B. D. Mouse germ line stem cells undergo rapid and stochastic turnover. *Cell Stem Cell* **7,** 214–224 (2010).
25. Rompolas, P. *et al.* Live imaging of stem cell and progeny behaviour in physiological hair-follicle regeneration. *Nature* **487,** 496–499 (2012).
26. Ritsma, L. *et al.* Surgical implantation of an abdominal imaging window for intravital microscopy. *Nature Protocols* **8,** 583–594 (2013).
27. Ritsma, L. *et al.* Intravital microscopy through an abdominal imaging window reveals a pre-micrometastasis stage during liver metastasis. *Sci. Transl. Med.* **4,** 158ra145 (2012).
28. Tian, H. *et al.* A reserve stem cell population in small intestine renders Lgr5-positive cells dispensable. *Nature* **478,** 255–259 (2011).
29. Rompolas, P., Mesa, K. R. & Greco, V. Spatial organization within a niche as a determinant of stem-cell fate. *Nature* **502,** 513–518 (2013).
30. Kozar, S. *et al.* Continuous clonal labeling reveals small numbers of functional stem cells in intestinal crypts and adenomas. *Cell Stem Cell* **13,** 626–633 (2013).

Supplementary Information is available in the online version of the paper.

Acknowledgements The authors would like to thank A. de Graaff from the Hubrecht Imaging Center for imaging support, all members of the van Rheenen group for useful discussions and the Hubrecht Institute animal caretakers for animal support. This work was supported by a Vidi fellowship (91710330; J.v.R.) and equipment grants (175.010.2007.00 and 834.11.002; J.v.R.) from the Dutch Organization of Scientific Research (NWO), a grant from the Dutch Cancer Society (KWF; HUBR 2009-4621; J.v.R.), a grant from the Association for International Cancer Research (AICR; 13-0297; J.v.R.), and the Wellcome Trust (grant number 098357/Z/12/Z; B.D.S.).

Author Contributions J.v.R. and L.R. conceived the study. L.R. optimized the surgical and imaging procedure. L.R., S.I.J.E., A.Z. and H.J.S. performed imaging experiments. L.R., H.J.S., B.D.S. and S.I.J.E. performed analyses. F.J.d.S. provided the $Lgr5^{DTR:eGFP}$ mice and B.D.S. did all biophysical modelling. L.R. and S.I.J.E. made the figures. J.v.R. and H.C. supervised the study. All authors discussed results and participated in preparation of the manuscript.

Author Information Reprints and permissions information is available at www.nature.com/reprints. The authors declare no competing financial interests. Readers are welcome to comment on the online version of the paper. Correspondence and requests for materials should be addressed to J.v.R. (j.vanrheenen@hubrecht.eu) or H.C. (h.clevers@hubrecht.eu).

METHODS

Mice. All experiments were carried out in accordance with the guidelines of the Animal Welfare Committee of the Royal Netherlands Academy of Arts and Sciences. To obtain Lgr5$^{eGFP\text{-}Ires\text{-}CreERT2}$/R26R-Confetti mice, R26R-Confetti[7] mice were crossed with Lgr5$^{eGFP\text{-}Ires\text{-}CreERT2}$ mice[1]. Random double heterozygous male mice between 10 and 22 weeks old were used for experiments. Three days before imaging, mice were injected with 2.5–5 mg tamoxifen (single injection; Sigma Aldrich) to induce activation of Cre recombinase, which in turn induced expression of one of the Confetti colours (membranous CFP, cytoplasmic YFP and RFP). Nuclear GFP was also activated, but that subset of Confetti-labelled cells was not followed. For the targeted ablation studies, four male Lgr5$^{DTR:eGFP}$ mice with an AIW received 50 μg kg^{-1} DT through intraperitoneal injections. Depletion of Lgr5^{+} cells was confirmed by intravital imaging. Mice in which Lgr5^{+} cells were not completely depleted after 24 h received a second DT injection. Mice were housed under standard laboratory conditions and received food and water *ad libitum*.

AIW surgery. The AIW surgery was performed as described previously[26]. In short, all surgical procedures were performed under 2% isoflurane (v/v) inhalation anaesthesia. Before surgery, buprenorphine (3 μg per mouse; Temgesic, BD Pharmaceutical Systems) was administered intramuscularly. The left lateral flank of the mice was shaved and the skin was disinfected with 70% (v/v) ethanol. Next, a left lateral flank incision was made through the skin and abdominal wall and a purse string suture was placed along the wound edge. A disinfected AIW (>1 h in 70% (v/v) ethanol) was placed glass-side down next to the mice and the ileum was placed on top. 3 M Vetbond Tissue Adhesive (*n*-butyl cyanoacrylate) was used to fix the ileum to the cover glass of the AIW and CyGel (BioStatus Limited) was added to diminish peristaltic movement. After 5 min the AIW was inverted and placed in the mouse, with the skin and abdominal wall placed inside the AIW groove. Then the sutures were tightened to stably secure the window into the animal. After surgery the mice were provided with food and water *ad libitum*. Furthermore, mice were closely monitored once a day before imaging for behaviour, reactivity, appearance and defecation.

Equipment and settings. Intravital imaging was performed on an inverted Leica TCS SP5 AOBS two-photon microscope with a chameleon Ti:Sapphire pumped optical parametric oscillator (Coherent) equipped with a ×25 (HCX IRAPO NA0.95 WD 2.5 mm) water objective and four non-descanned detectors (NDDs). The NDDs collect the following wavelengths: NDD1, <455 nm; NDD2, 455–490 nm; NDD3, 500–550 nm; NDD4, 560–650 nm. Sequential scanning was performed, exiting the tissue with 860 and 960 nm wavelengths. The Confetti colours were detected as follows: 860 nm, NDD2 (CFP and eGFP); 960 nm, NDD3 (eGFP and YFP), NDD4 (YFP and RFP). Second harmonic generation (SHG) signal was generated by 960 nm excitation at collagen I and detected in NDD2. Scanning was performed in a bidirectional mode at 700 Hz and 12 bit, with a zoom of 1.7, 512 × 512 pixels. z-stacks with 2.5 μm z-steps of typically 70–80 images were acquired. Re-identification of the same crypts over multiple days was accomplished by storing the *xy* coordinates of the imaged regions using the 'multiple position' function in the LAS-AF software and using the vasculature and the typical (Confetti) Lgr5^{+} crypt pattern as visual landmarks.

Multi-day intestinal stem-cell imaging. After placing the AIW, mice were kept under anaesthesia and placed face-down in a custom-designed imaging box in which isoflurane (1% (v/v)) was administered through a facemask as described previously[26]. For the multi-day imaging sessions (Figs 1c, d, 2, 3b, 4 and Extended Data Figs 1, 2, 4, 5, 7), mice were imaged once a day for a maximum of 3 h, during which the climate chamber surrounding the microscope was kept at 32 °C. After the imaging session the mice were allowed to wake up to maintain their body temperature. After imaging, acquired z-stacks were corrected for *z* and *xy* shifts using a custom-designed Visual Basic software program and further processed and analysed using basic functions in ImageJ software (linear contrasting, blurring, median filtering).

Short-term intestinal stem-cell imaging. Mice were anaesthetized using isoflurane (2% (v/v)). The left lateral flank was shaved and the skin was disinfected using 70% (v/v) ethanol. Next, a left lateral flank incision was made through the skin and abdominal wall and the ileum was extracorporated using in PBS-drowned cotton swabs. The ileum was placed on a custom-designed inset containing a coverslip fitting the custom-designed imaging box. The ileum was secured to the coverslip using Vetbond and CyGel. The mouse was placed on top of the intestine and PBS-drowned sterile cotton gauzes were placed next to the animal to prevent dehydration. ParafilmM (Sigma Aldrich) was used to cover the mouse and a subcutaneous infusion system was used to provide 100 μl of sterile PBS per hour. The inset was placed within the custom-designed imaging box in which isoflurane (1% (v/v)) was administered through a facemask as described earlier. The temperature of the mouse was monitored during imaging using a rectal probe and was kept between 36 and 37 °C by adjusting the temperature of the surrounding climate chamber. Imaging was performed every 2 h for 14 h. z-stacks with a z-step of 2.5 μm of 12 regions with on average 6 crypts were made. Acquired z-stacks were analysed using ImageJ plugins (TurboReg, 3D visualization, 3D viewer).

Intravital imaging of Lgr5^{+}-cell-depleted mice. Mice with an AIW received 50 μg kg^{-1} DT through intraperitoneal injections. Depletion of Lgr5^{+} cells was confirmed by intravital imaging. Mice in which Lgr5^{+} cells were not completely depleted after 24 h received a second DT injection. Only mice in which full depletion was confirmed by intravital imaging 24 h after the last DT injection were analysed. The number of Lgr5^{+}–GFP cells within the stem-cell niche border and centre was determined as described in Fig. 1b.

Real-time lineage tracing of clonal competition. The data from the lineage tracing were collected at random, and all clones that were imaged with a 3-day interval were included. The strength of a Confetti-labelled Lgr5^{+} CBC cell to produce offspring was expressed as the fold increase in Confetti-labelled Lgr5^{+} CBC cell number 3 days after the first imaging session. A Mann–Whitney U test was performed because the data were not normally distributed.

Quantitative data analysis of multi-day lineage tracing. Lineage tracing was performed for 80 clones in 80 crypts from 4 mice. No sample size estimate was calculated before the study was executed. Only data from mice from which high enough quality images were acquired were included in the study. The number of Confetti-labelled cells per crypt position (centre (rows 0 to +2), border (rows +3 to +4), TA (rows >4)) was scored. From the 80 lineages, we obtained 33 sublineages originating from the central region (Fig. 4a), and 47 sublineages from the border (Fig. 4b).

Immune cell analysis on intestinal tissue. Six E-Cadherin-CFP/Lgr5$^{eGFP\text{-}Ires\text{-}CreERT2}$ mice, 22 weeks of age, were randomly divided into two groups: a control and a window group to test potential side effects of AIWs. AIWs were implanted on top of the small intestines of mice from the window group, whereas mice from the control group did not undergo surgery. After 24 h, all mice were killed and the small intestines were harvested. Note that in the window group the part of the small intestine that was located directly behind the window was harvested. The small intestines were fixed for 1 day in fixation mix (1% paraformaldehyde, 0.2% $NaIO_4$, 61 mM Na_2HPO_4, 75 mM L-Lysine and 14 mM NaH_2PO_4 in H_2O). After fixation, the tissues were placed for 6 h into 30% sucrose after which the tissues were snap-frozen using Tissue Freezing Medium (Leice Microsystems Nussloch GmbH). Sixteen-micrometre sections were cut using a Leica CM3050 cryotome. A standard immunohistochemistry protocol was used to stain the sections with CD45 antibodies (BD Pharmingen, 553078, Clone 30-F11) and random areas were imaged. For analysis, ten areas within the imaged regions were selected and analysed in a blinded manner. The number of CD45-positive cells within a region was counted manually and an averaged number for each mouse was calculated. Next, the average of the three mice per group was calculated. A Mann–Whitney U test was performed because the sample was not distributed normally, and no significant differences were found. The variance between the groups was tested with an F-test, and was not different.

Clone frequency window versus control mice. Eight Lgr5$^{eGFP\text{-}Ires\text{-}CreERT2}$ mice, 22 weeks of age, were divided into two groups: a control and a window group. All mice received 5 mg tamoxifen by intraperitoneal injection. Three days later, AIWs were implanted on top of the small intestines of mice from the window group, whereas mice from the control group did not undergo surgery at this point. Two days after the surgery (5 days after tamoxifen injection) all mice were imaged. In the control group the intestine was exteriorized before imaging (as described earlier). In the window group the mice were imaged through the AIW. Several random areas were imaged. All recorded clones were used for analysis. For a single clone the number of cells within the stem-cell compartment was determined and a frequency distribution was made for the two groups.

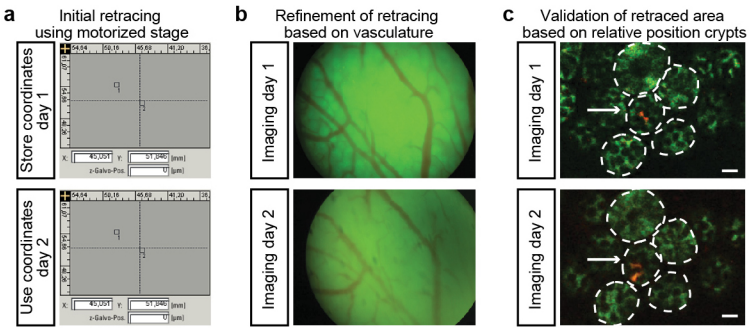

Extended Data Figure 1 | Retracing of the intravital imaging fields. **a**, The coordinates of the imaging fields within the imaging window (which always has a fixed position within the stage) were stored. By applying these stored coordinates in the subsequent imaging sessions, we recovered the same positions. **b**, The vasculature was used to refine the retracing. **c**, The retraced imaging areas were validated based on the relative position of the coloured crypts. Scale bars, 20 μm.

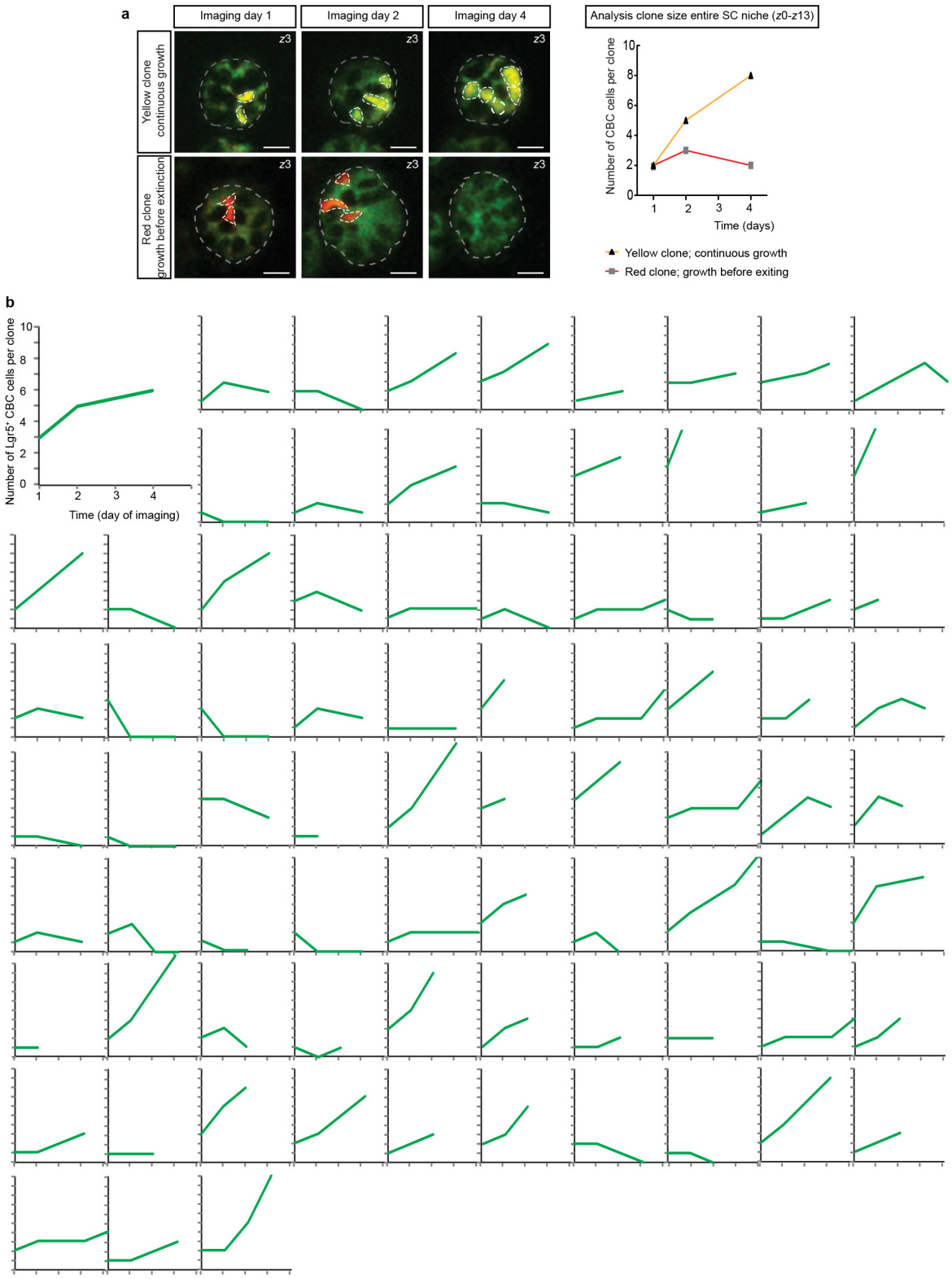

Extended Data Figure 2 | Real-time lineage tracing of individual clones. **a**, Expression of a Confetti colour was induced in Lgr5$^+$ CBC cells, and their progeny was followed over time. Two examples of Confetti-labelled Lgr5$^+$ CBC cells expanding over time are shown to illustrate clonal competition at indicated times. The top images show the continuous expansion of a YFP-expressing Lgr5$^+$ CBC cell (yellow line) in the central region of the crypt. The bottom images show the size of a clone derived from an RFP-expressing Lgr5$^+$ CBC cell in the central region of the crypt, which first increases and then declines (red line). The Confetti-labelled cells are outlined by a white dashed line and the crypts by a grey dashed line. Scale bars, 20 μm. Right, graph shows the increase in the number of YFP- or RFP-expressing Lgr5$^+$ CBC cells in the entire stem-cell compartment of the crypts shown in the images on the left (yellow and red line, respectively). **b**, A total of 80 crypts were imaged in four mice. The total clone size (border and central) of Confetti$^+$ cells present in the stem-cell niche independent of Lgr5 expression (row 0 to +4, which translates to z0 to z13 of the z-stack) was analysed at the indicated times ($n = 4$ mice) for all 80 lineages. The first time point translates to several days after induction. Every graph represents one crypt.

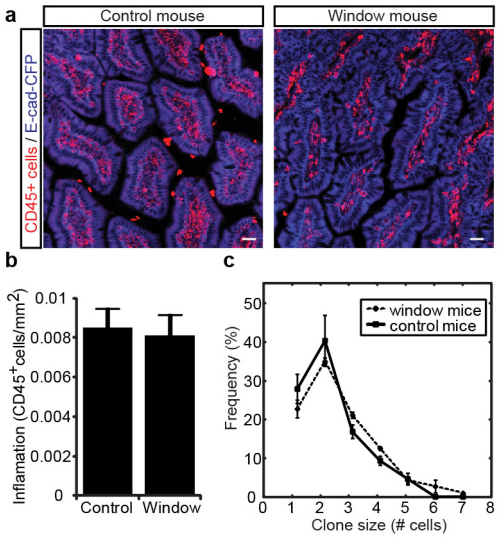

Extended Data Figure 3 | Clonal dynamics are unaffected by AIW surgery. **a**, Abdominal imaging windows (AIW) were surgically implanted into the abdominal wall of E-Cadherin-CFP/Lgr5$^{eGFP\text{-}Ires\text{-}CreERT2}$ mice. To detect CD45^{+} immune cells, tissue sections of the small intestine of these and control (no AIW) mice were stained with CD45 antibodies. Scale bar, 20 µm. **b**, Quantification of images in **a**. Regions of interest within the stromal area of the small intestines were measured and the number of CD45^{+} cells was counted within those regions. The bars show averages and s.e.m. ($n = 10$ regions per mouse performed in 3 mice per condition). **c**, Five days after tamoxifen injection, the clones of Lgr5$^{eGFP\text{-}Ires\text{-}CreERT2}$/R26R-Confetti mice were imaged intravitally. In control mice, the intestine was exteriorized before imaging and, in window mice, a window was placed 2 days before imaging. The frequency of clones with a certain size is plotted in the graph. The lines show the mean and s.e.m. ($n = 4$ mice per condition).

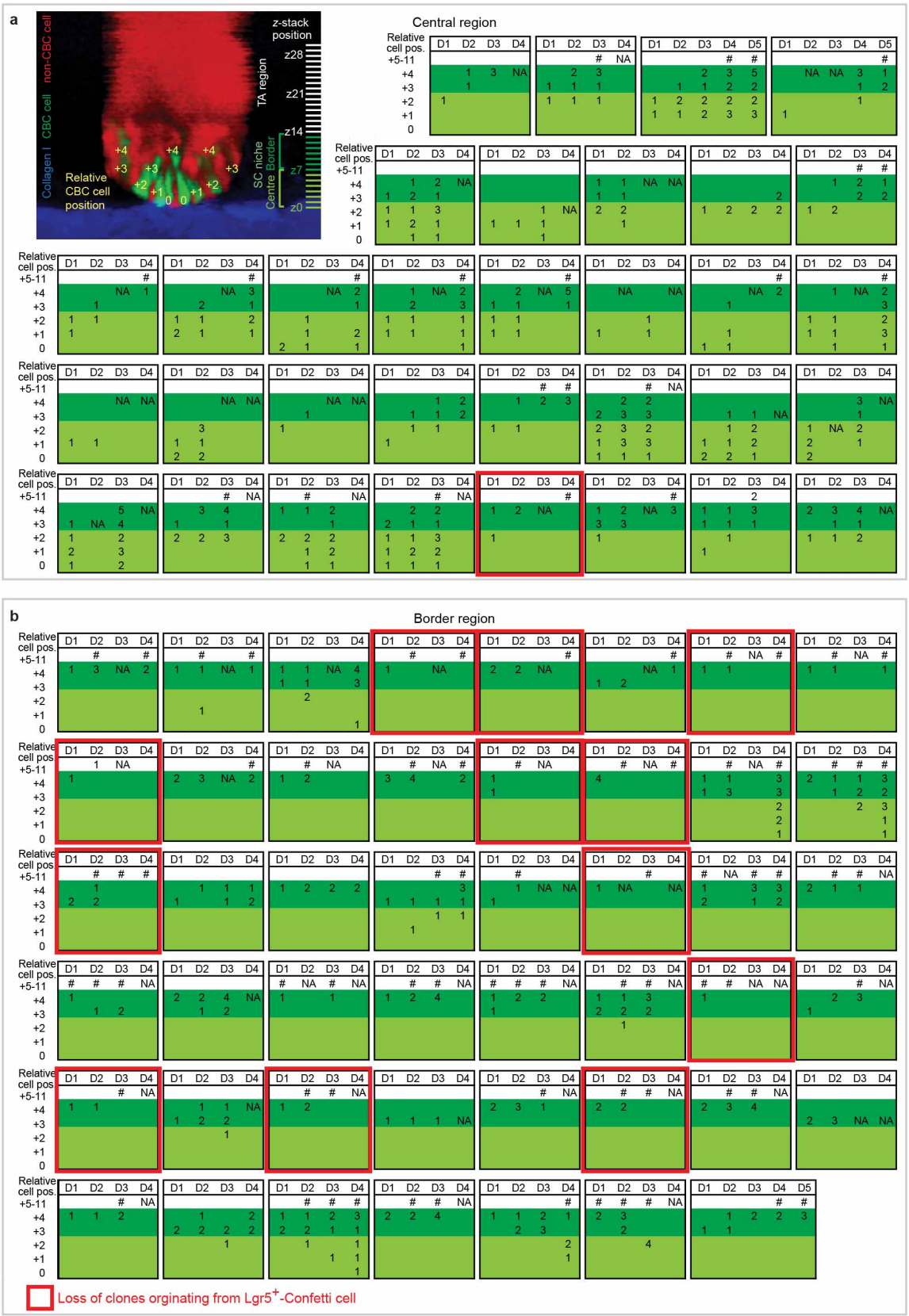

Extended Data Figure 4 | The spatial distribution of Confetti clone expansion within the stem-cell niche. **a**, **b**, Spatial distribution of confetti clones, subdivided into clones starting in the central (**a**) or border (**b**) region ($n = 4$ mice). Top left panel (**a**) shows the relative Confetti^{+} cell position within the stem-cell niche, where row 0 to +4 translates to z0 to z13 of the z-stack. Every table shows the number of Confetti-labelled cells that are present at the different positions in the crypt, independent of Lgr5 expression. The position within the central and border region of the stem-cell niche and TA compartment are colour coded. The hash symbol indicates the presence of Confetti-labelled cells in the TA compartment. NA indicates time points for which data was not available owing to crypts that were not retraceable at that specific time point.

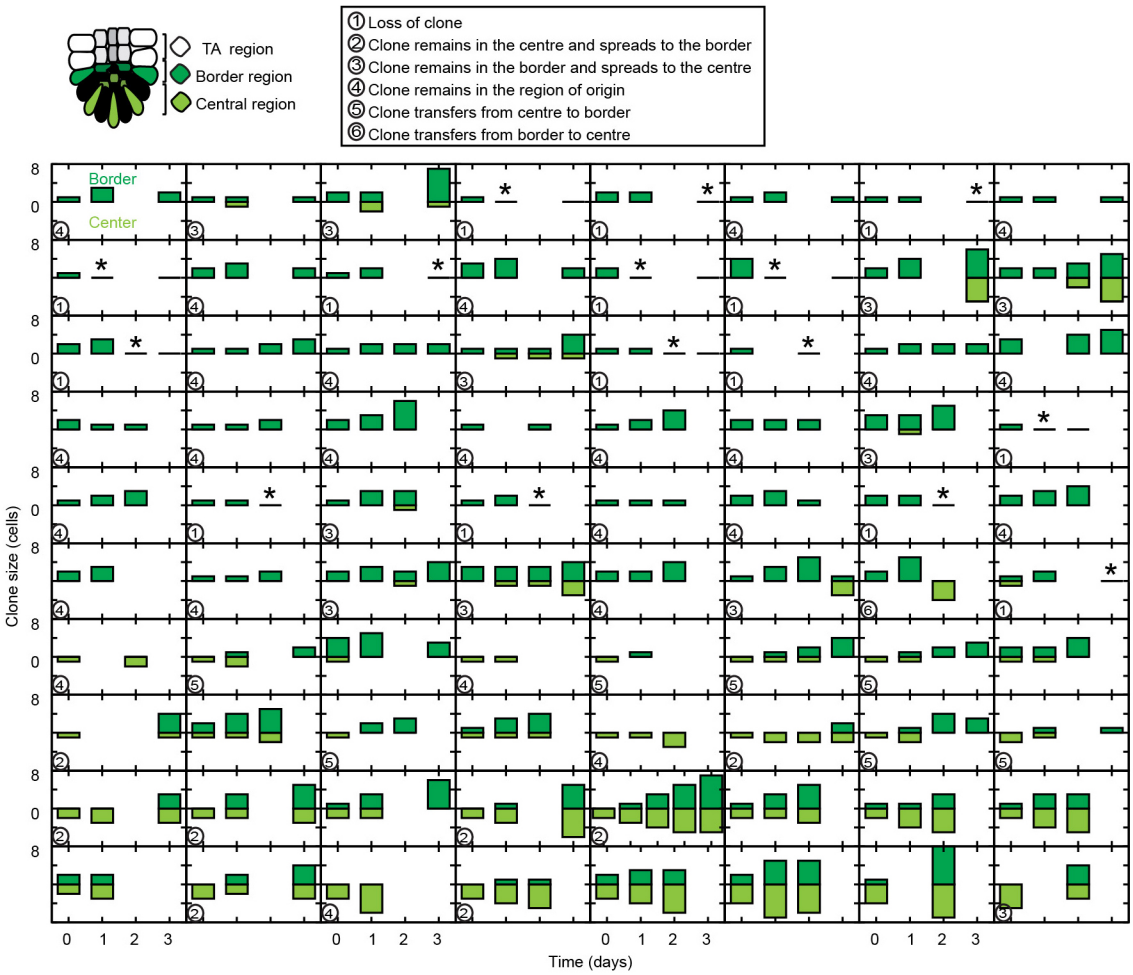

Extended Data Figure 5 | Average clone size and survival probability. Cartoon shows the division of the intestinal stem-cell niche into a central and border region. The central region contains rows 0 to +2, which translates to z0 to z6 of the z-stack, and the border region contains rows +3 and +4, which translates to z7 to z13 of the z-stack (see Fig. 1b). Confetti expression was induced in Lgr5^{+} CBC cells. The panels show, at the indicated time, the spatial organization of the 80 lineages of progeny of the Confetti-labelled CBC cells (same clones as in Extended Data Figs 2, 4) ($n = 4$ mice). For each lineage, we recorded the number of cells per clone in the central and border regions of the stem-cell niche at the indicated times. The first time point translates to several days after induction. The asterisks indicate clones in which all progeny were lost from the niche region.

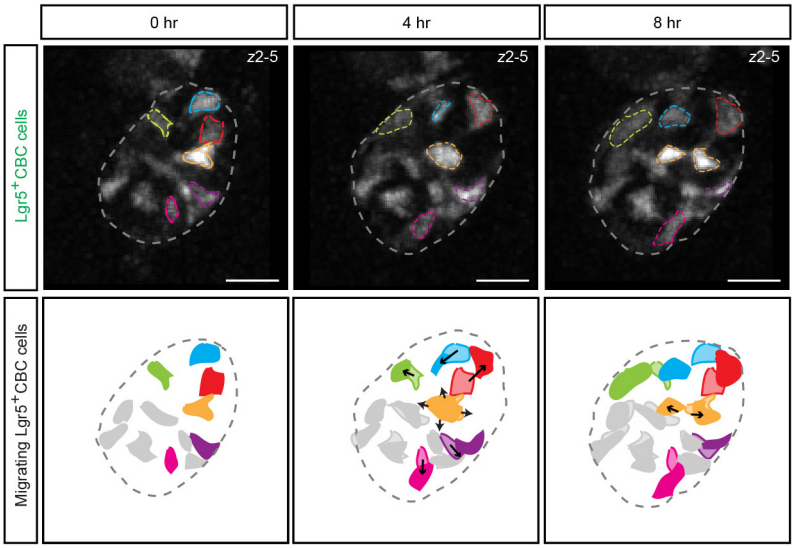

Extended Data Figure 6 | Lgr5$^+$ CBC cells move and can become expelled from the stem-cell niche. Top, maximum projection images (z2 to z5) of a time series of a crypt. In the lower cartoons, the Lgr5$^+$ CBC cells are highlighted. The moving cells are indicated with a different colour. The location of the cells at earlier time points are shown by a lighter colour and arrows indicate the direction of movement. Scale bars, 20 µm.

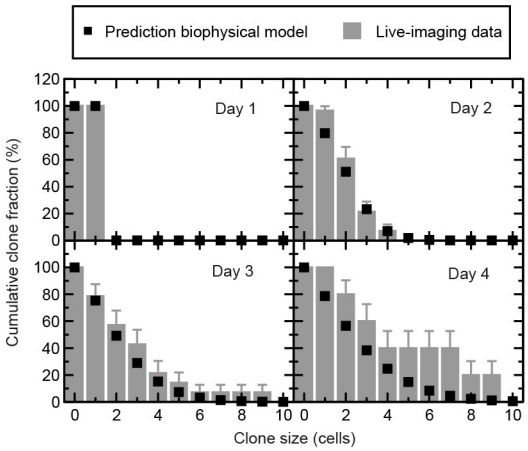

Extended Data Figure 7 | Cumulative clone size distributions derived from two border mother cells. Cumulative clone size distributions of clones derived from two neighbouring cells in the border region. In each case, the size of the clone is defined by the total number of constituent cells in the central and border regions (rows 0 to +4), independent of GFP expression. Note that the cumulative clone size distribution records the fraction of clones that have a size larger than the given value. The bars represent measurements from individual lineages reconstructed from live imaging at days 1 (**a**, $n = 13$; **b**, $n = 35$; **c**, $n = 35$), 2 (**a**, $n = 10$; **b**, $n = 25$; **c**, $n = 28$), 3 (**a**, $n = 7$; **b**, $n = 14$; **c**, $n = 14$) and 4 (**a**, $n = 6$; **b**, $n = 8$; **c**, $n = 6$). Error bars denote s.e.m. The points represent the predictions of the biophysical model using the same parameters as those inferred from the short-term live-imaging assay (for details, see Fig. 3a and Supplementary Notes).

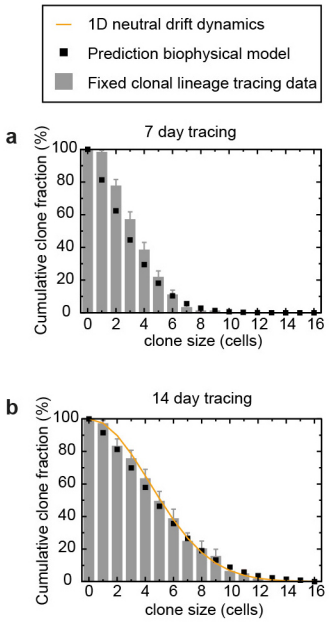

Extended Data Figure 8 | Longer-term clonal evolution and the approach to scaling behaviour. **a**, **b**, Cumulative clone size distribution at 7 days (**a**) and 14 days (**b**) after induction, showing the percentage of clones that have a constituent number of $Lgr5^+$ CBC cells larger than the given value. For example, the data point at around four cells (40%) in **a** shows that, at 7 days post-induction, some 40% of clones have a size larger than four $Lgr5^+$ cells, and so on. The bars reproduce the findings of a fixed clonal assay using the same Lgr5-Confetti mouse construct used in the present study and previously described[7]. Error bars denote s.e.m. Points represent the predictions of the biophysical model using the same parameters as those inferred from the short-term live-imaging assay (see Fig. 3 and Supplementary Notes). To account for the prolonged activity of Cre recombinase in the static clonal assay, in both cases we introduced a 1-day time delay. At the 14-day time point, the measured clone size distribution and model prediction are beginning to converge onto the universal scaling behaviour characteristic of a strictly one-dimensional neutral drift dynamics (line) (for details, see Supplementary Notes).

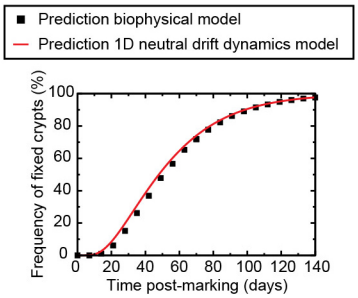

Extended Data Figure 9 | Long-term drift towards monoclonality of labelled crypts. Predicted frequency of monoclonal crypts over time expressed as a percentage of surviving clones after pulse labelling of stem cells at clonal density. Points show the predictions of the biophysical model defined in the main text and Supplementary Notes using the same parameters as those inferred from the short-term live-imaging assay (see Fig. 3 and Supplementary Notes) after the representative marking of stem cells at the crypt base, and the line shows the predictions of the strictly one-dimensional neutral drift dynamics model introduced previously[8], with a stem-cell loss replacement rate of 0.24 per day and a total of 8 stem cells. The convergence of these two model predictions at longer times shows that, first, the behaviour of the quasi-one-dimensional model approaches that of the strictly one-dimensional model at longer times and, second, that the effective loss/replacement rate and stem-cell number in the new model is essentially fixed by the rate $P_{cc}\lambda = 0.24$ per day and the eight stem cells that occupy the central region. Significantly, these parameters translate to the ratio $P_{cc}\lambda/N_{stem}{}^2 = 0.026$ per week, very close to the figure of 0.025 per week obtained from a fit of the measured monoclonal crypt fraction to the one-dimensional neutral drift dynamics model in ref. 8. (For the labelling protocol and the experimental data points, we refer to the original reference.)